International Journal of Fracture, Vol. 14, No. 1, February 1978
Sijthoff & Noordhoff International Publishers
Alphen aan den Rijn, The Netherlands

An analysis of the crack tip stress field in DCB adhesive fracture specimens

S. S. WANG

University of Illinois, Urbana, Illinois 61801, *USA*

J. F. MANDELL and F. J. McGARRY

Massachusetts Institute of Technology, Cambridge, Massachusetts 02139, *USA*

(Received January 7, 1977; in revised form July 20, 1977)

ABSTRACT

The problem of a cracked adhesive bonded DCB-type fracture specimen has been analyzed using a hybrid stress model finite element analysis which incorporates an advanced crack tip element. Stresses in the near and far fields have been studied as a function of adherend/adhesive modulus ratio and adhesive thickness. The results are compared to monolithic systems with regard to the stress intensity factor and the localization of the singular stress domain associated with the crack tip.

1. Introduction

The propagation of cracks in structural adhesive joints is a significant fracture problem for which little theoretical development is available. The characteristics of the stress field in the adhesive and adherend near the crack tip have been difficult to obtain even for elastic behavior due to the complexity introduced by the singular nature at the crack tip and the discontinuous material properties. Numerical solutions are further complicated by the vast disparity in moduli and dimensions between the gross adherend boundaries and the region across the adhesive layer thickness where the stress distribution must be accurately described.

In contrast to the theoretical complications, the special characteristics of adhesive bonded systems lead to relatively simple techniques of fracture toughness testing. The most common type of fracture test specimen is the double cantilever beam (DCB) type [1, 2]. In this test, adherend beams (usually metallic) are bonded together with the adhesive, and the crack is propagated along the adhesive layer in the opening mode by pin loading at the beam ends (Fig. 1). The usual problem of the colinear propagation of the crack common in monolithic materials is not as significant in the adhesive system, and nonlinear effects are limited to the adhesive layer. Cracks usually propagate in a cohesive mode, although some cases of adhesive (interface) propagation have been reported [1]. Data from the test are reduced by beam theory or an experimental calibration to give the critical strain energy release rate [3]. A similar test specimen using tapered beams to obtain an approximately linear compliance at various crack lengths is now recommended by ASTM [4].

The interest in the adhesive fracture problem and the widespread use of fracture mechanics techniques to characterize the toughness have lead to a more detailed study of the stress distribution in the crack tip region. This paper describes an elastic analysis which uses the hybrid stress finite element model and incorporates an advanced crack tip superelement. Results are given for the case of a crack in the center-of-bond plane of a DCB specimen, but the analysis is not limited to symmetric problems.

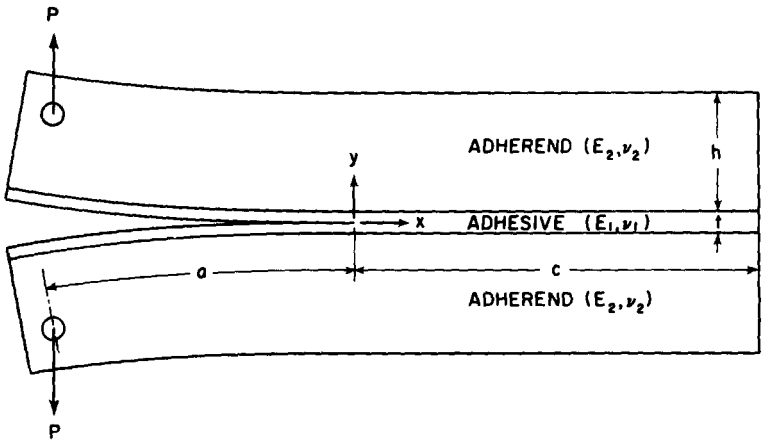

Figure 1. Double cantilever beam (DCB).

2. Formulation of the analysis

2.1. *General formulation*

The hybrid stress approach of the finite element method, pioneered by Pian [5, 6], is characterized by the use of an assumed stress field in the element and an assumed displacement field along element boundaries. The formulation of the analysis is based on the minimum complementary energy principle (a modified complementary energy functional is used in the formulation of the crack tip superelement). Additional features of the method are flexibility of formulation, selection of elements and expedient achievement of interelement compatibility. More accurate solutions and faster convergence rates than those of conventional displacement models can be obtained. The singular behavior of the crack tip region, which is critical to the fracture problem, can be exactly modeled in the formulation without an increase in the number of elements. The complex geometric variables and multiphase materials effects are also conveniently taken into account.

The hybrid stress finite element method procedure is specialized for application to the current plane crack problem by the introduction of a crack tip superelement within which the singular stress behavior is considered by properly selected stress functions. This assumed stress hybrid model for the problem was first introduced by Pian [5], and later refined by Tong, *et al.* [7] by the use of the complex variable formulation of Muskhelishvili stress functions. The general formulation of the procedure is given here for the case of the plane crack problem in a DCB adhesive joint. The formulations for the crack tip superelement and its surrounding regular (non-singular) hybrid elements have been described in detail elsewhere [5, 7], and only a brief outline is given here.

Consider a crack of length a, as described in Fig. 1. The complementary energy functional of the whole domain of the specimen (after dividing into a finite number of discrete elements) may be expressed as

$$\Pi_c = \Pi_m + \sum_i \Pi_r^{(i)} \tag{1}$$

where Π_m is referred to the crack tip superelement and $\Pi_r^{(i)}$ to the ith regular surrounding element in the given domain. Applying the variational energy principle to the functional Π_c, one obtains

$$\Pi_c = \sum_n \left[\frac{1}{2} \boldsymbol{q}_n^T \boldsymbol{k}_n \boldsymbol{q}_n - \boldsymbol{q}_n^T \bar{\boldsymbol{Q}}_n \right] \tag{2}$$

where

$$\boldsymbol{k}_n = \boldsymbol{G}_n^T \boldsymbol{H}_n^{-1} \boldsymbol{G}_n$$

represents the general form of the element stiffness matrix, and is calculated in different ways in the crack tip superelement and the surrounding regular elements as described in the next section. The equivalent nodal force $\bar{\boldsymbol{Q}}_n$ is defined as

$$\bar{\boldsymbol{Q}}_n = \boldsymbol{G}_n^T \boldsymbol{\beta}_n \tag{3}$$

The matrices, $\boldsymbol{G}_n$, $\boldsymbol{H}_n$ and $\boldsymbol{\beta}_n$ are defined in following sections in detail.

Assembling all the element stiffness matrices together, a set of linear equations of the form

$$\boldsymbol{K}\boldsymbol{q} = \boldsymbol{Q} \tag{4}$$

is established. The displacement field can be solved by a standard Gauss–Cholosky elimination scheme

$$\boldsymbol{q} = \boldsymbol{K}^{-1} \boldsymbol{Q} \tag{5}$$

The stress parameters $\boldsymbol{\beta}_n$ for the nth element are then calculated from

$$\boldsymbol{\beta}_n = \boldsymbol{H}_n^{-1} \boldsymbol{G}_n \boldsymbol{q}_n \tag{6}$$

The associated stress field at the location (x_p, y_p) of interest can be obtained from

$$\boldsymbol{\sigma}(x_p, y_p) = \boldsymbol{P}(x_p, y_p) \boldsymbol{H}_n^{-1} \boldsymbol{G}_n \boldsymbol{b}_n \boldsymbol{q}_n \tag{7}$$

where $\boldsymbol{b}_n$ is a Boolean transformation.

2.2. *Superelement formulation*

The conventional displacement model and non-singular hybrid stress element have difficulty handling the crack problem even in a monolithic material, since the use of high order polynomials as interpolation functions does not improve the rate of convergence for this kind of problem. The reason for this is that the convergence rate of the finite element method is controlled by the nature of the solution in the singular region [7]. However, the use of the complex variable technique in the hybrid element formulation permits proper consideration of the stress singularity and of higher order effects in the crack tip region, and it leads to highly accurate results with a relatively coarse mesh.

The modified complementary energy functional, Π_m, is used for the crack tip superelement. Consider a plane elasticity problem with prescribed boundary traction $\bar{T}_i$ over the boundary s_σ and prescribed displacement $\tilde{u}_i$ over the boundary s_u. The functional is defined in the form

$$\Pi_m = \int_{\partial A_m} (\tilde{u}_i - u_i) T_i \, \mathrm{d}s - \int_{(s_\sigma)_m} u_i \bar{T}_i \, \mathrm{d}s + \frac{1}{2} \iint_{A_m} [\sigma_{ij}(u_{i,j} + u_{j,i}) - S_{ijkl}\sigma_{ij}\sigma_{kl}] \, \mathrm{d}A \tag{8}$$

The Euler equations for this functional are

$$\frac{1}{2}(u_{i,j} + u_{j,i}) = S_{ijkl}\sigma_{kl} \tag{9}$$

$$\sigma_{ij,j} = 0 \tag{10}$$

Following Muskhelishvili's formulation [8], the stress and displacement fields in the plane elasticity problem can be expressed in terms of two stress functions $\phi(Z)$ and $\psi(Z)$ of the complex variable Z as

$$\sigma_{yy} + \sigma_{xx} = 2[\phi'(Z) + \overline{\phi'(Z)}]$$
$$\sigma_{yy} - \sigma_{xx} + 2i\sigma_{xy} = 2[\bar{Z}\phi''(Z) + \psi'(Z)] \tag{11}$$

and

$$2G(u + iv) = \eta\phi(Z) - Z\overline{\phi'(Z)} - \overline{\psi(Z)}$$

where both $\phi(Z)$ and $\psi(Z)$ are analytical in the Z-plane, and $G = E/2(1 + \nu)$ with

$$\eta = (3 - \nu)/(1 + \nu) \quad \text{for plane stress} \tag{12}$$

or

$$\eta = (3 - 4\nu) \quad \text{for plane strain} \tag{13}$$

In order to choose proper stresses and displacements for the crack element which would account for possible singularities of all order, as well as higher order terms, the following mapping function is introduced

$$Z = w(\zeta) = \zeta^2 \tag{14}$$

with

$$-\pi/2 \leq arg\zeta \leq \pi/2$$

Thus, on the ζ-plane the stress functions $\phi(\zeta)$ and $\psi(\zeta)$ are analytical functions of ζ. Using this mapping function, Eqn. (11) becomes

$$\sigma_{yy} + \sigma_{xx} = 4\,\mathrm{Re}[\phi'(\zeta)/w'(\zeta)]$$
$$\sigma_{yy} - \sigma_{xx} + 2i\sigma_{xy} = 2\{\overline{w(\zeta)}[\phi'(\zeta)/w'(\zeta)]' + \psi'(\zeta)\}/w'(\zeta) \tag{15}$$

and

$$2G(u + iv) = \eta\phi(\zeta) - w(\zeta)\overline{\phi'(\zeta)}/\overline{w'(\zeta)} - \overline{\psi(\zeta)}$$

By imposing the traction free boundary condition ($T_x = T_y = 0$) on the crack surfaces, as

$$i\int_s (T_x + iT_y)\,ds = 0 = \phi(Z) + Z\overline{\phi'(Z)} + \psi(Z) \tag{16}$$

$\psi(\zeta)$ can be calculated from $\phi(\zeta)$

$$\psi(\zeta) = -\overline{\phi(-\bar{\zeta})} - \overline{w(-\bar{\zeta})}\phi'(\zeta)/w'(\zeta) \tag{17}$$

In constructing the superelement stiffness matrix, $\phi(\zeta)$ is assumed to have the form

$$\phi(\zeta) = \sum^{N} b_j\zeta^j \tag{18}$$

Thus, from Eqn. (17) we have

$$\psi(\zeta) = -\sum^{N} [\bar{b}_j(-1)^j + \frac{j}{2}b_j]\zeta^j \tag{19}$$

where

$b_j = \beta_j + i\beta_{N+j}$ (non-symmetric case)

$b_j = \beta_j$ (symmetric case)

with the β's being real constants.

Substituting Eqns. (18) and (19) back into Eqn. (15), the stresses and displacements can be explicitly expressed in terms of ζ as

$$\sigma_{xx} - i\sigma_{xy} = \sum^{N} \left\{ \mathrm{Re}(j\zeta^{j-2}) - \left[\frac{(j-2)}{4}\frac{\bar{\zeta}^2}{\zeta^2} - \frac{j}{4} - \frac{1}{2}(-1)^j\right] j\zeta^{j-2} \right\} \beta_j + \sum^{N} \left\{ -\mathrm{Im}(j\zeta^{j-2}) - i\left[\frac{(j-2)}{4}\frac{\bar{\zeta}^2}{\zeta^2} - \frac{j}{4} + \frac{1}{2}(-1)^j\right] j\zeta^{j-2} \right\} \beta_{N+j} \tag{20a}$$

$$\sigma_{yy} + i\sigma_{xy} = \sum^{N} \left\{ \mathrm{Re}(j\zeta^{j-2}) + \left[\frac{(j-2)}{4}\frac{\bar{\zeta}^2}{\zeta^2} - \frac{j}{4} - \frac{1}{2}(-1)^j\right] j\zeta^{j-2} \right\} \beta_j + \sum^{N} \left\{ -\mathrm{Im}(j\zeta^{j-2}) + i\left[\frac{(j-2)}{4}\frac{\bar{\zeta}^2}{\zeta^2} - \frac{j}{4} + \frac{1}{2}(-1)^j\right] j\zeta^{j-2} \right\} \beta_{N+j} \tag{20b}$$

and

$$2G(u+iv) = \sum^{N} \left\{ \left[\eta\zeta^j + (-1)^j\bar{\zeta}^j\right] - \frac{1}{2} j\bar{\zeta}^{j-2}(\zeta^2 - \bar{\zeta}^2) \right\} \beta_j + i\sum^{N} \left\{ [\eta\zeta^j + (-1)^j\bar{\zeta}^j] + \frac{1}{2} j\bar{\zeta}^{j-2}(\zeta^2 - \bar{\zeta}^2) \right\} \beta_{N+j} \tag{20c}$$

From Eqns. 20(a, b, and c) one can express the boundary tractions and interior displacements as

$$\begin{aligned} \boldsymbol{T} &= \boldsymbol{R}\boldsymbol{\beta}_c \\ \boldsymbol{u} &= \boldsymbol{U}\boldsymbol{\beta}_c \end{aligned} \tag{21}$$

where $\boldsymbol{\beta}_c$ is a column vector with its components being $\beta_1, \beta_2, \ldots \beta_{2N}$. The boundary displacement $\tilde{\boldsymbol{u}}$ shall be assumed in terms of generalized nodal displacement $\boldsymbol{q}$ as

$$\tilde{\boldsymbol{u}} = \boldsymbol{L}\boldsymbol{q} \tag{22}$$

A substitution of Eqns. (21) and (22) into Eqn. (8) and taking variation of the functional Π_m with respect to $\boldsymbol{\beta}_c$ yields the crack element stiffness matrix $\boldsymbol{k}_c$

$$\boldsymbol{k}_c = \boldsymbol{G}^T\boldsymbol{H}^{-1}\boldsymbol{G} \tag{23}$$

and

$$\boldsymbol{\beta}_c = \boldsymbol{H}^{-1}\boldsymbol{G}\boldsymbol{q} \tag{24}$$

where

$$\boldsymbol{H} = \frac{1}{2}\int_{\partial A_m} (\boldsymbol{U}^T\boldsymbol{R} + \boldsymbol{R}^T\boldsymbol{U})\, ds$$

$$\boldsymbol{G} = \frac{1}{2}\int_{\partial A_m} \boldsymbol{R}^T\boldsymbol{L}\, ds$$

After obtaining the displacement field of the system by solving the assembled global stiffness matrix $\boldsymbol{K}$, the stress field in the superelement can be calculated from Eqns. 20(a, b and c). The stress intensity factors K_{I} and K_{II} can be related to $\boldsymbol{\beta}_c$ by

$$\begin{bmatrix} K_{\mathrm{I}} \\ K_{\mathrm{II}} \end{bmatrix} = \sqrt{2\pi} \begin{bmatrix} \beta_1 \\ \beta_{N+1} \end{bmatrix} \tag{25}$$

2.3. *Regular hybrid stress element formulation*

The complementary energy functional to be varied for the regular element is given by

$$\Pi_r^{(m)} = \iint_{A_m} \frac{1}{2} \boldsymbol{\sigma}^T \boldsymbol{S} \boldsymbol{\sigma} \, dA - \int_{Su_m} \bar{\boldsymbol{u}}^T T \, ds \tag{26}$$

Along each boundary of the element, an assumed displacement field is selected, and expressed in terms of the nodal displacements $\boldsymbol{q}$

$$\bar{\boldsymbol{u}} = \boldsymbol{L}\boldsymbol{q} \tag{27}$$

where $\boldsymbol{L}$ is the interpolation function. The stresses in the interior of the element are expressed by undetermined stress parameters $\boldsymbol{\beta}$

$$\boldsymbol{\sigma} = \boldsymbol{P}(x, y)\boldsymbol{\beta} \tag{28}$$

where $\boldsymbol{P}$ is chosen to satisfy the homogenous equilibrium equation

$$\sigma_{ij,j} = 0 \tag{29}$$

The surface tractions, which are related to the stress components by $T_i = \sigma_{ij} n_j$, can be written in the form

$$\boldsymbol{T} = \boldsymbol{R}\boldsymbol{\beta} \tag{30}$$

Substituting Eqns. (27), (28) and (30) into (26), the functional $\Pi_r^{(m)}$ becomes

$$\Pi_r^{(m)} = \frac{1}{2} \boldsymbol{\beta}^T \boldsymbol{H} \boldsymbol{\beta} - \boldsymbol{\beta}^T \boldsymbol{G} \boldsymbol{q} \tag{31}$$

where

$$\boldsymbol{H} = \iint_{A_m} \boldsymbol{P}^T \boldsymbol{S} \boldsymbol{P} \, dA$$

$$\boldsymbol{G} = \int_s \boldsymbol{R}^T \boldsymbol{L} \, ds$$

Taking the variation of the functional $\Pi_r^{(m)}$ with respect to the stress parameters $\boldsymbol{\beta}$ to minimize the complementary energy, the element stiffness matrix can be obtained as

$$\boldsymbol{k}_r = \boldsymbol{G}^T \boldsymbol{H}^{-1} \boldsymbol{G} \tag{32}$$

3. Accuracy of the analysis

The accuracy and convergence of the analysis are complicated by several unusual features of the problem and of the crack tip superelement. As mentioned earlier, the finite element mesh must accommodate both the small dimension of the adhesive thickness and the larger dimensions of the remainder of the specimen, a difference of three orders of magnitude. It is essential to model the adhesive layer and the crack tip region accurately with a number of elements across the adhesive thickness so that the high stress gradient within the adhesive layer may be discerned. This geometric characteristic combines with the extreme difference in adhesive and adherend elastic moduli to cause significant numerical round-off errors, so double precision mode was required for accurate solutions.

Optimization of the mesh discretization is also complicated by the differences between the crack tip superelement and the surrounding elements. The superelement

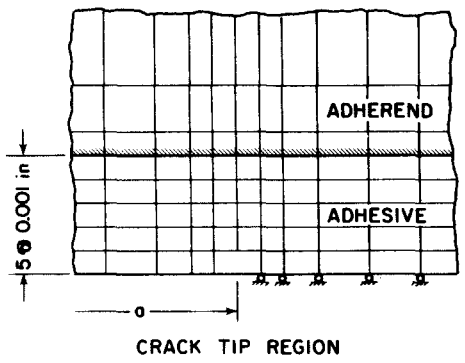

Figure 2. Typical FEM mesh near the crack tip.

gives an exact stress distribution, and it is advantageous to use as large a crack tip superelement as possible. On the other hand, the regular elements surrounding the crack tip must be sufficiently small to give accurate results in the domain beyond the superelement, which also is of interest. As a result, a compromise must be reached which yields an accurate solution both very close to the crack tip and in the surrounding region which also gives the minimum band width for the stiffness matrix. Arrangement of the mesh must also satisfy the geometric constraint that the crack tip superelement be embedded in the adhesive layer, and that the number of degrees of freedom of the entire system be minimum in terms of computer run time.

A study of the accuracy and convergence of the analysis has been made using test cases for which independent solutions are available in the literature. Figures 3 and 4 give the convergence of the solution for the double-edge-cracked tension configuration previously analyzed by Bowie [9]. Figure 3 indicates that convergence of the

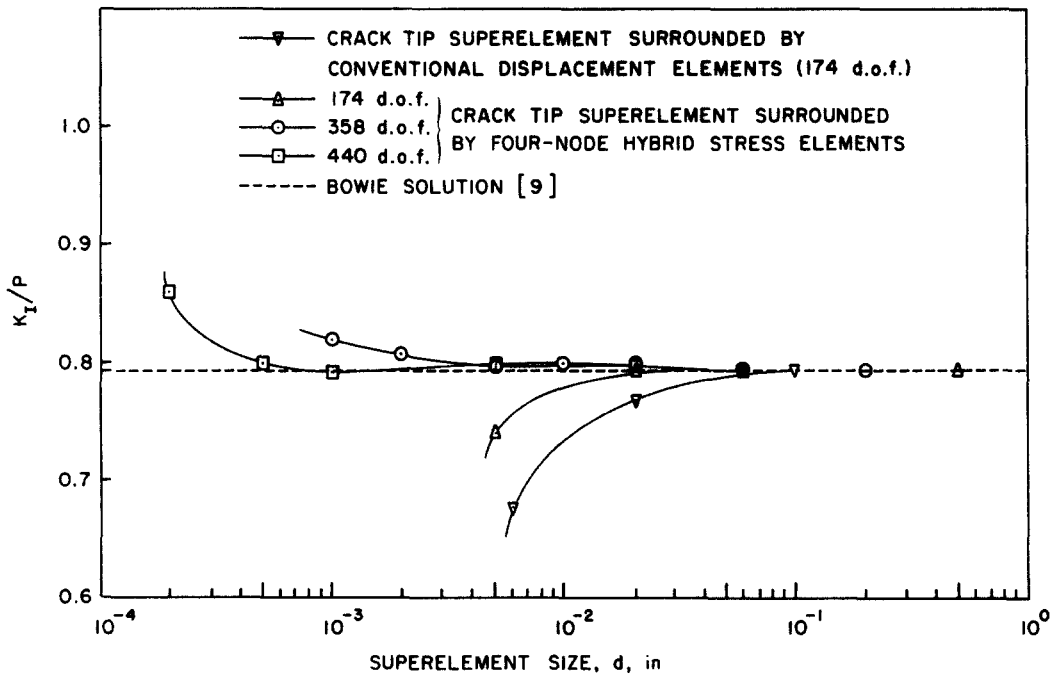

Figure 3. Effect of crack tip superelement size on stress intensity factor for various elements and mesh configurations.

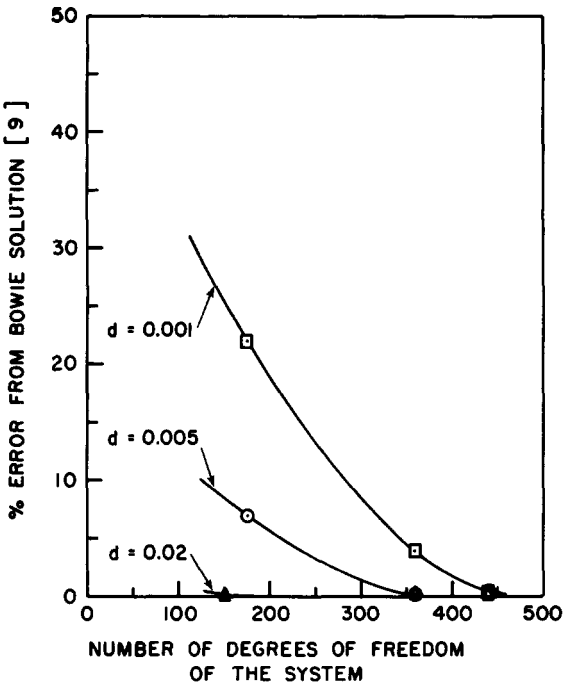

Figure 4. Error *vs.* number of degrees of freedom for three superelement sizes.

solution is slower for smaller crack tip superelement sizes, but that satisfactory convergence can be obtained even with superelement dimensions significantly less than 10^{-3} in if surrounding non-singular elements have compatible sizes. Typically, the accuracy of the converged solution is within one percent of Bowie's solution. This figure also demonstrates the superiority of the hybrid stress elements relative to conventional displacement elements for the domain beyond the superelement. Figure 4 further defines the total number of degrees of freedom necessary to obtain convergence for various superelement dimensions.

Figure 5 compares the results of Kanninen [10] for the monolithic DCB-type

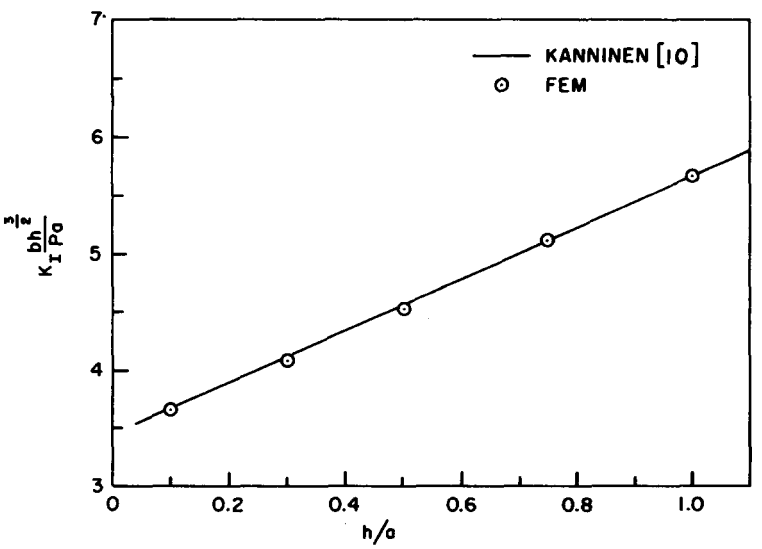

Figure 5. Comparison of current analysis and Kanninen's solution (homogeneous material).

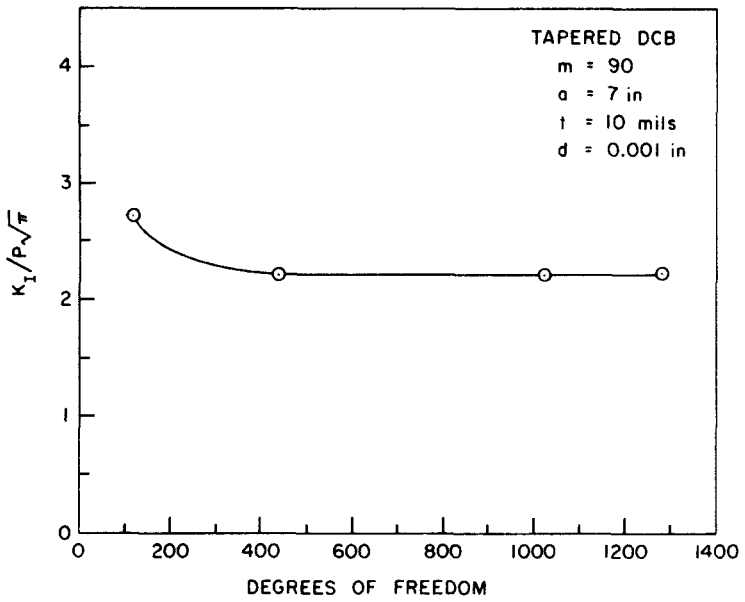

Figure 6. Convergence of solution for TDCB adhesive specimen for various mesh breakdowns.

specimen with results from the present analysis. The two solutions are in good agreement over a range of crack lengths.

Due to a lack of existing solutions, it was not possible to test the analysis against other results for adhesive crack problems. However, the convergence of the solution has been tested for various mesh configurations, as indicated in Fig. 6. This figure clearly demonstrates that the solution converges to within one percent for a broad range of degrees of freedom above 400. These results are for one of the most difficult cases from the viewpoint of numerical analysis (the tapered DCB specimen with a shape factor, m, of $90\,\text{in}^{-1}$, and a crack length of 7.0 in). The ratio of adherend to adhesive elastic modulus for this case is 20, a typical value. Results for the straight-sided specimen would not differ significantly from those in Fig. 6.

The data of Figs. 3–6 and other results obtained in the course of development of the analysis clearly indicate that a solution may be obtained which is within approximately one percent of the exact solution if the proper superelement size and mesh configuration are maintained. Figure 2 represents a typical mesh configuration in the crack tip region; mesh configurations of this type are sufficiently fine to give an accurate representation of the full stress field around the crack tip as well as in regions removed from the crack tip. The exact solution obtained within the superelement for a given loading on its boundary enables a meaningful test of the type and extent of singular behavior for distances arbitrarily close to the crack tip. The superelement size and mesh configuration used to obtain the results in the following sections in all cases are well within the limits of convergence of the analysis.

4. Results

This section describes the elastic stress distribution near the crack tip for several adhesive moduli and thicknesses. While these results refer to the DCB specimen with a specific crack length of 2.0 in, and beam height, h, of 0.5 in, they represent the character of the stress field found for cases of opening mode adhesive cracks with specimens of this general type. Changes in specimen shape or crack length only serve to alter the intensity of the stress field or the scale of the stresses and distances, but

not the essential character of the distributions. The specific effects of specimen shape and crack length will be considered elsewhere. Figure 1 gives the coordinates and dimensions of the problem. The parameters considered are the normal stresses σ_{xx} and σ_{yy}, the in-plane shear stress σ_{xy} and the stress intensity factor for the near crack tip region, K_I. The results obtained from the analysis are normalized by the applied load P and are for a unit width specimen. The moduli of the adhesive and adherend in the analytical work are taken as a ratio, E_2/E_1, the Young's modulus ratio of adherend to adhesive. If the adherend is aluminum, a modulus of approximately 10^7 psi is appropriate. This gives an E_2/E_1 ratio of 20 to 40 for typical epoxy adhesives, but a broader modulus range is considered in most cases for purposes of generality.

4.1. *Loading of the adhesive and effects of modulus ratio*

Figure 7 gives the displacement in the y-direction of the adhesive-adherend interface in the region of the crack tip. This figure illustrates the shape into which the beam deforms for various modulus ratios. Comparison of the distortions for the monolithic case ($E_2/E_1 = 1$) with those for the softer adhesive systems is informative in characterizing the general nature of the problem in the crack tip region. When the adhesive is relatively soft, the beam displacements do not reflect any severe disturbance at the crack tip but gradually decrease over a long distance ahead of it. While the curvature of the beam does reverse at this point in response to the loading of the now continuous adhesive, the rapid closure evident in the monolithic case just ahead of the crack tip is not present. As will be clear from the following, this is indicative of the fact that the beams do not experience a high gradient crack tip stress field, since the singular region becomes localized within the adhesive layer.

It is evident from Fig. 7 that the deformation and traction on the adhesive layer is dictated by the displacement pattern of the relatively stiff beams along the interface.

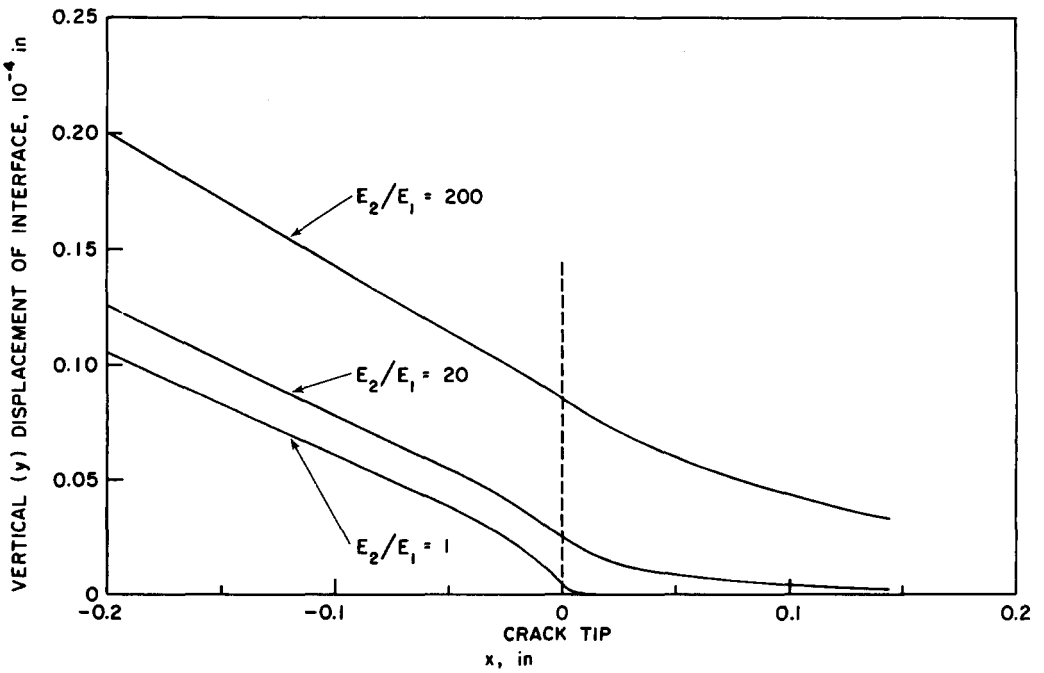

Figure 7. Bending shape of beam at interface, DCB, $a = 2.0$ in, $P = 1.0$ lb.

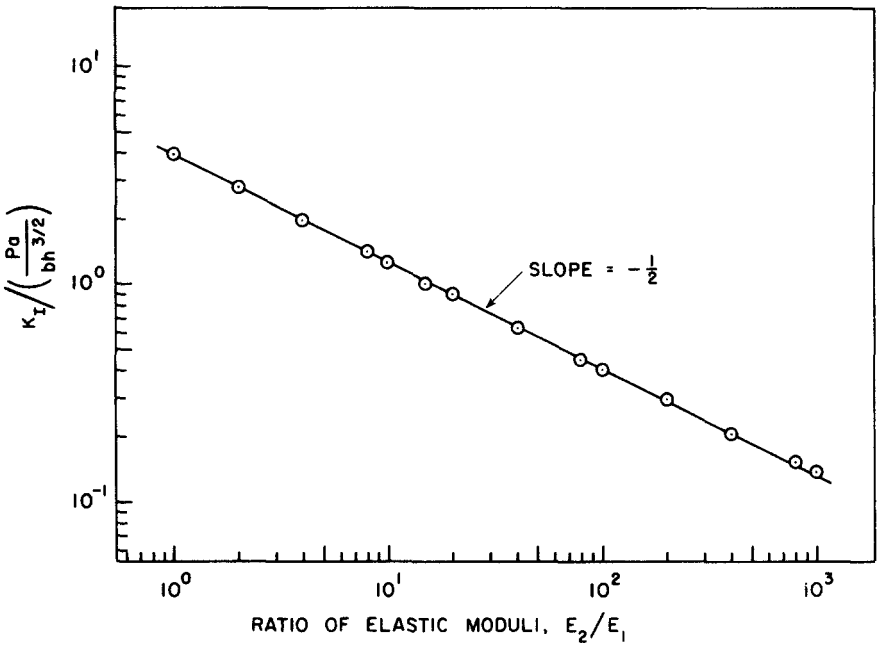

Figure 8. Effect of the ratio of elastic moduli on the stress intensity factors (straight-sided DCB specimen).

In the region of the crack tip, the beams impose a slowly varying displacement for a distance of many adhesive layer thicknesses each way. The softer the adhesive is relative to the adherend, the greater is the displacement imposed by the beam, and the longer is the region over which the significant displacement occurs ahead of the crack. The stress intensity factor determined at the crack tip in the adhesive is a function of the loading by the beam and of the modulus ratio. Figure 8 gives the stress intensity factor in the adhesive as a function of modulus ratio over a broad range. The data are well described on the log-log plot by a straight line with a slope of $-1/2$.

4.2. *K–G relationship in the adhesive system*

The K–G relationship is of concern in the adhesive system due to the possibility that the constraint of the adherend could disturb the local crack tip response. This is particularly true for the thin adhesive layer/long crack geometry considered here. The results plotted in Fig. 8 provide some confirmation of the relationship between K_I and the strain energy release rate, G_I, for the adhesive system according to the following line of reasoning:

1. The value of G_I is determined primarily by the beam geometry and modulus for the DCB specimen. It may be calculated approximately from beam theory including the shear effect [11] as

$$G_I = \frac{4P^2}{E_2}\left(\frac{3a^2}{h^3}+\frac{1}{h}\right) \tag{33}$$

where P is the applied force. The value of G_I is relatively insensitive to the presence of the adhesive.

2. K_I, the stress intensity factor in the adhesive, is calculated from the finite element results. (There is no K_I in the beams, as will be discussed later.)

3. From Fig. 8, K_I^2 is proportional to E_1/E_2, and from Eqn. (33), G_I is

proportional to $1/E_2$. The relationship between K_I and G_I must then be of the form

$$G_I = f(E_1, E_2, \alpha)K_I^2 \tag{34}$$

where α is a geometric parameter.

4. The parameter f may be calculated from G_I and K_I (1 and 2) and Eqn. (34). The form of f is found to be

$$f(E_1, E_2, \alpha) = C\left(\frac{E_2}{E_1}\right)$$

where C is not a function of geometry. Results to be published for the tapered DCB specimen confirm the independence of the relationship from geometric factors for this class of specimens.

5. Substitution of f into Eqn. (34) gives

$$G_I = C\left(\frac{E_2}{E_1}\right)K_I^2$$

6. C may be evaluated from the monolithic case, $E_2/E_1 = 1$. The relationship for the monolithic case in plane stress is well known [12] as

$$G_I = \frac{K_I^2}{E_2}$$

so that

$$C = \frac{1}{E_2}$$

7. Thus, the $G_I - K_I$ relationship for adhesive bonded specimens of this general class is

$$G_I = \frac{K_I^2}{E_1} \tag{35}$$

The value of K_I in the adhesive can therefore be determined for the DCB-type specimen if the value of G_I is known from experimental calibration or from an analytical calibration for a monolithic system. Results reported by Trantina [13] suggest that this may hold for other specimen geometries as well if the adhesive layer is thin.

4.3. *Stresses near the crack tip*

Figures 9 and 10 give the peeling stress, σ_{yy}, along the x and y axes close to the crack tip. The stress distributions are similar to those that would be expected in a monolithic system, being dominated by the $1/\sqrt{r}$ singularity close to the crack tip, then deviating from singular behavior further away. However, the region over which the singular behavior dominates is greatly reduced in the adhesive systems ($E_2/E_1 > 1$) as compared to the monolithic ($E_2/E_1 = 1$). The stress close to the crack tip is reduced significantly as E_2/E_1 increases as expected from Fig. 8, but the inverse is true further from the crack tip as is necessary to satisfy force equilibrium. Deviation from the singular behavior occurs well within the crack tip element boundaries for the adhesive cases. Figure 10 indicates that the singular behavior extends well into the adherend region for $E_2/E_1 = 1$, but that there is no singular distribution in the adherend for higher modulus ratios; the entire singular domain being localized near the crack tip in the adhesive.

The fact that the effect of adhesive thickness on K_I is found to be negligible in

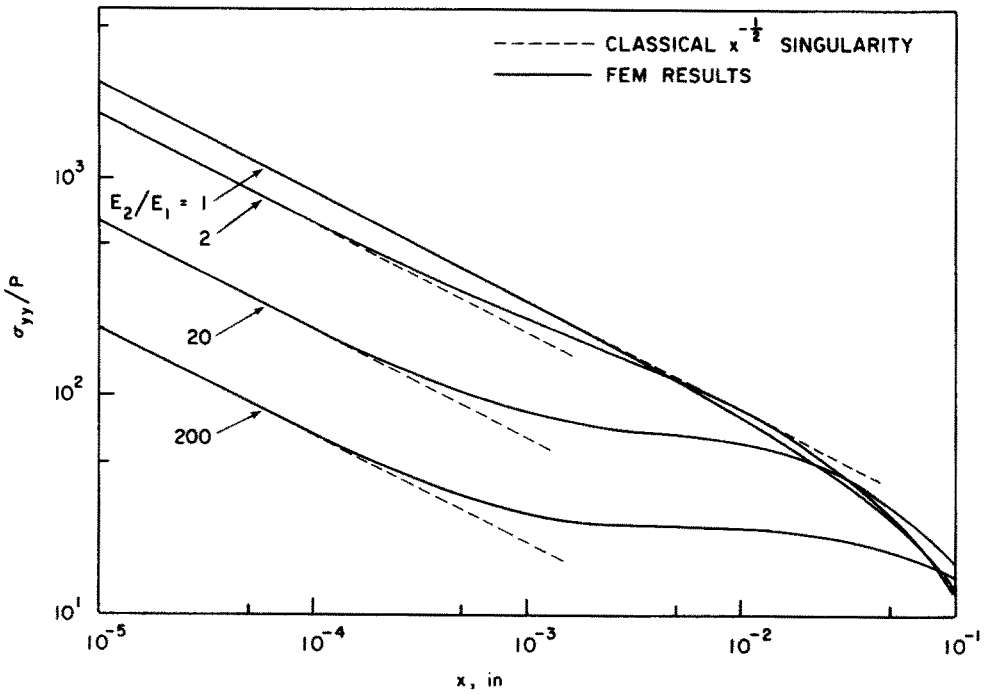

Figure 9. Effect of elastic modulus ratio on σ_{yy} ahead of crack tip, DCB, $a = 2.0$ in, $t = 0.010$ in.

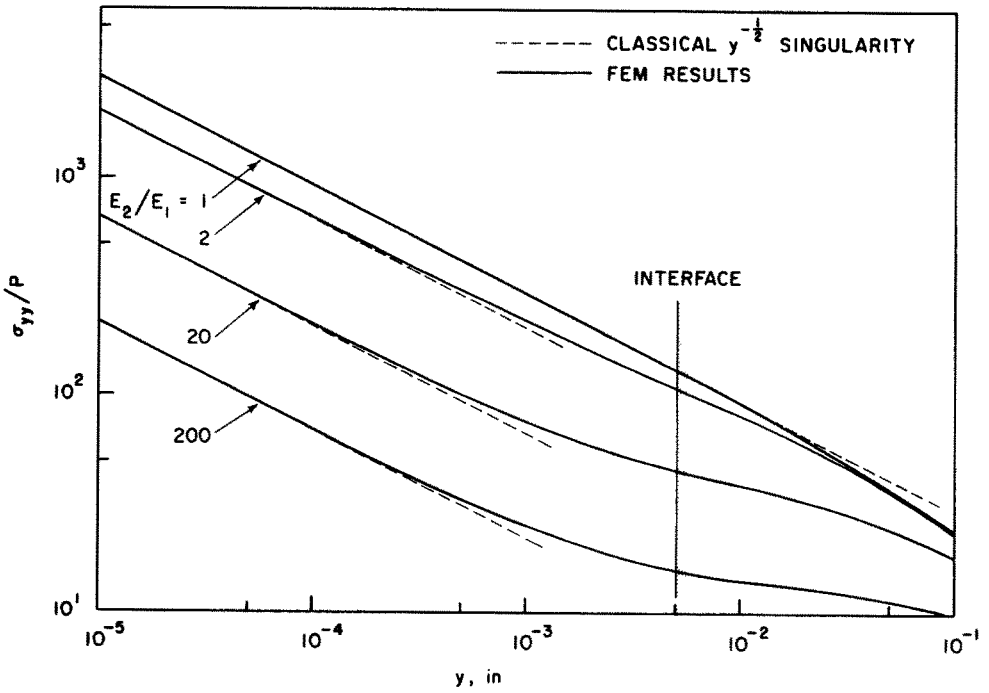

Figure 10. Effect of elastic modulus ratio on σ_{yy} along the y-axis, DCB, $a = 2.0$ in, $t = 0.010$ in.

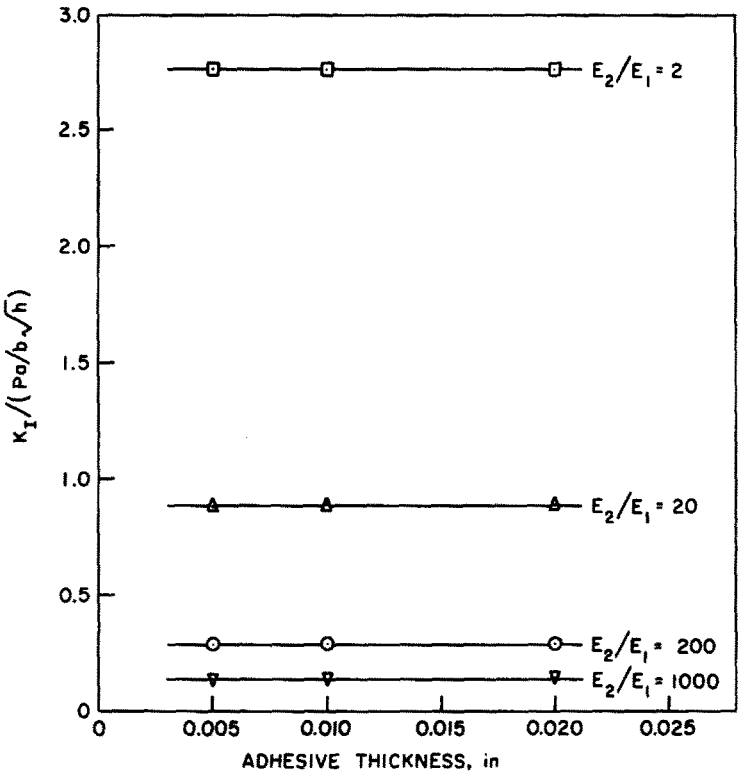

Figure 11. Effect of adhesive thickness on stress intensity factor for the DCB specimens with various elastic modulus ratios.

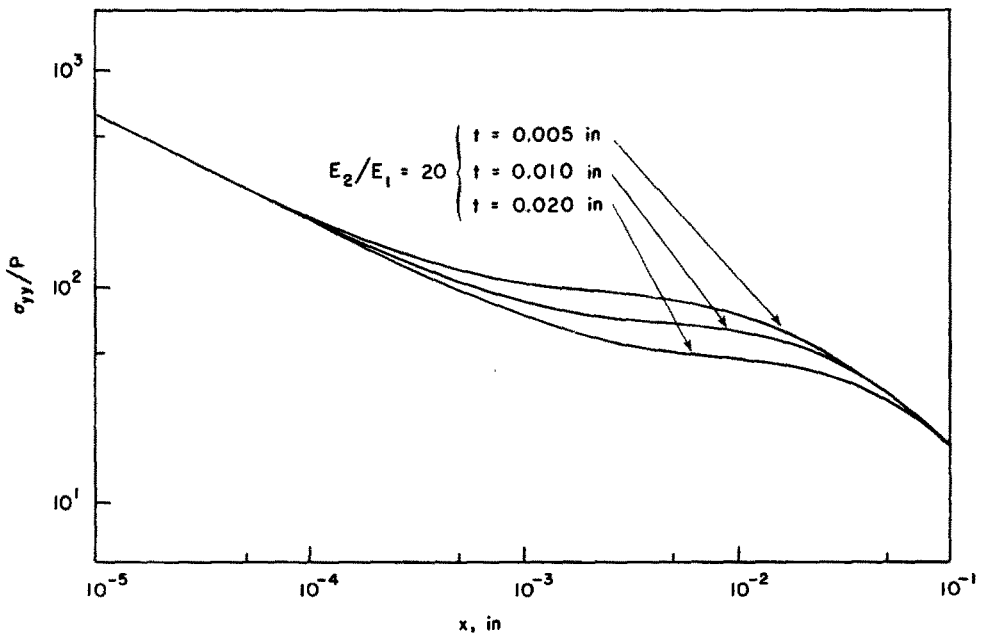

Figure 12. Effect of adhesive thickness on σ_{yy} along the x-axis, DCB, $a = 2.0$ in.

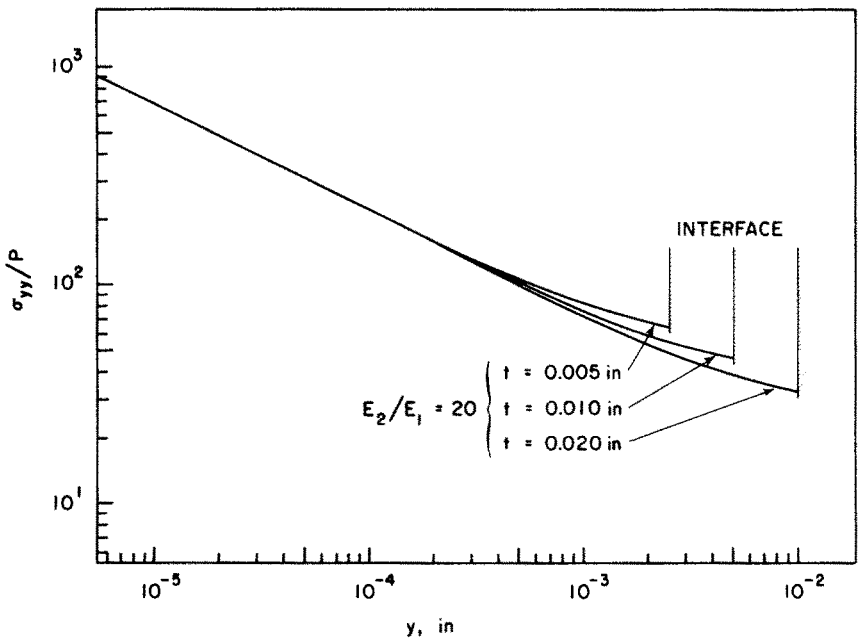

Figure 13. Effect of adhesive thickness on σ_{yy} along the y-axis, DCB, $a = 2.0$ in.

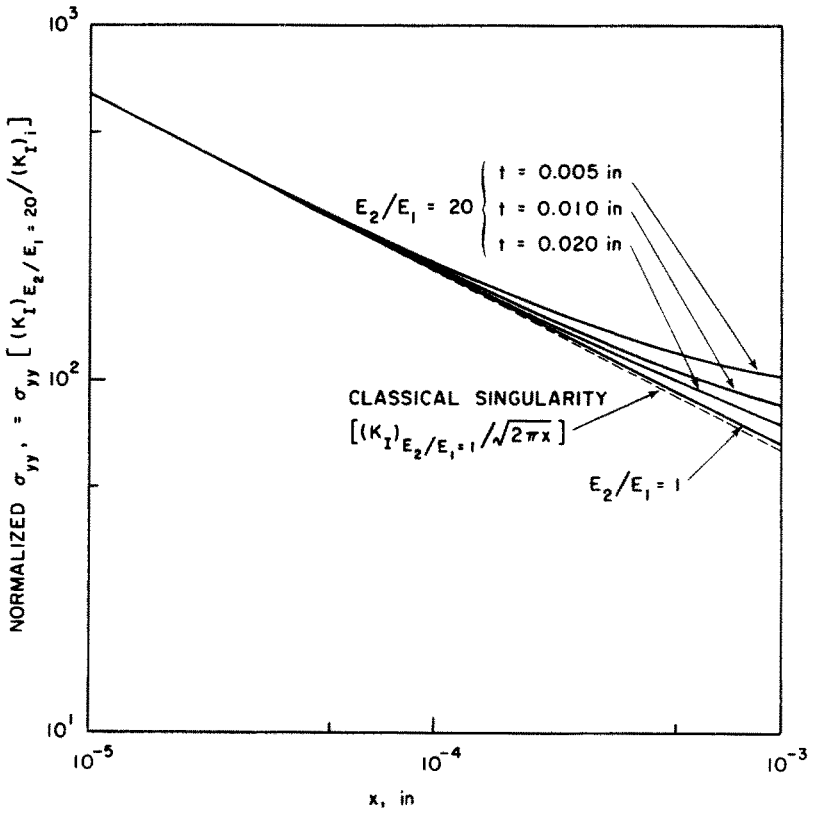

Figure 14. Deviation of σ_{yy} from classical singularity in near crack tip region, DCB, $a = 2.0$ in.

Fig. 11 for various modulus ratios (the beam height, h, is 0.50 in all cases) further confirms the characteristic of a very confined singular domain. The effect of thickness is more evident in Figs. 12 and 13, where significant differences in σ_{yy} are observed at small distances away from the crack tip despite convergence of the curves as the crack tip is approached and singular behavior becomes dominant.

The deviations from singular behavior are clearer on the expanded scale of Fig. 14. For the adhesive systems, the amount of deviation from singular behavior at a given value of x is greater for the thinner adhesives. The value of x at which a particular amount of deviation occurs is roughly proportional to the adhesive thickness. Returning to Fig. 9, it is also apparent that the value of x at which a particular amount of deviation occurs is not sensitive to the modulus ratio as long as $E_2/E_1 > 1$. These characteristics suggest that the extent of the domain which is dominated by singular behavior is governed by the adhesive thickness, whereas in monolithic systems, it is governed by the crack length or specimen dimensions. The value of x at which the stress deviates 10% from the singular relationship is approximately $t/40$ for the adhesive systems, but $h/33$ for the monolithic system, where $t = h/50$. The localization of the singular domain has certain implications for the limits of applicability of K_{IC} as fracture criterion which will be discussed elsewhere.

4.4. *Stresses in the far field*

Figure 15 gives the distribution of σ_{yy} further ahead of the crack tip, along the full length of the specimen. As anticipated from force equilibrium, the stress decreases and then becomes compressive at distances of several tenths of an inch ahead of the crack tip. The maximum compressive stress is only a small fraction of the tensile stresses closer to the crack tip.

Figures 16–18 give the variation of stresses σ_{yy}, σ_{xx} and σ_{xy}, respectively across the adhesive thickness and into the adherend at various distances ahead of the crack

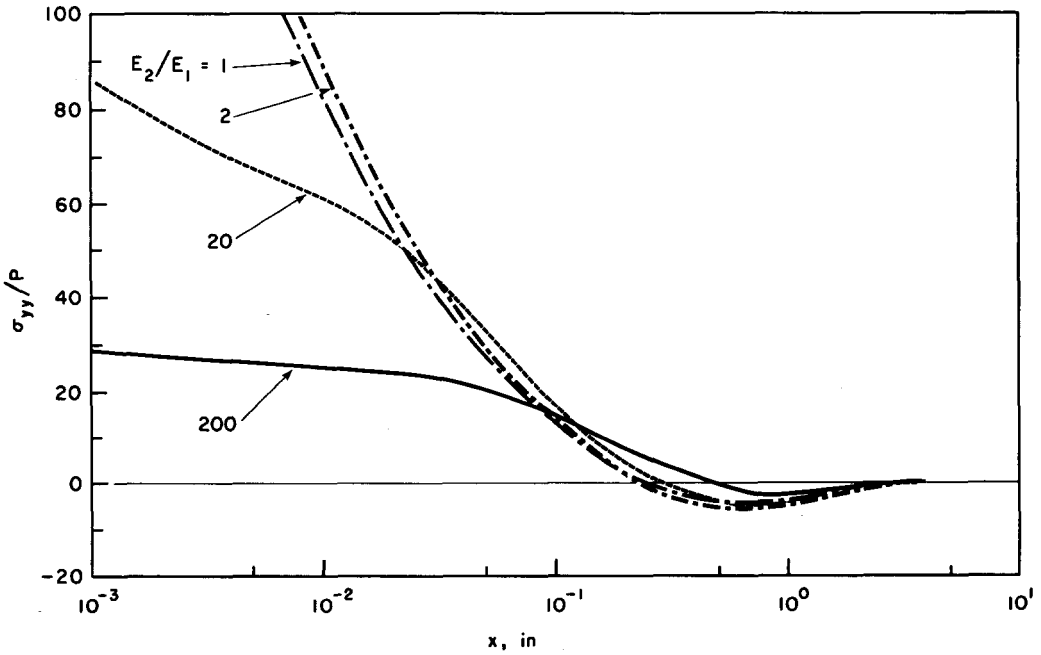

Figure 15. Distribution of σ_{yy} in the far field ahead of crack tip, DCB, $a = 2.0$ in, $t = 10$ mils.

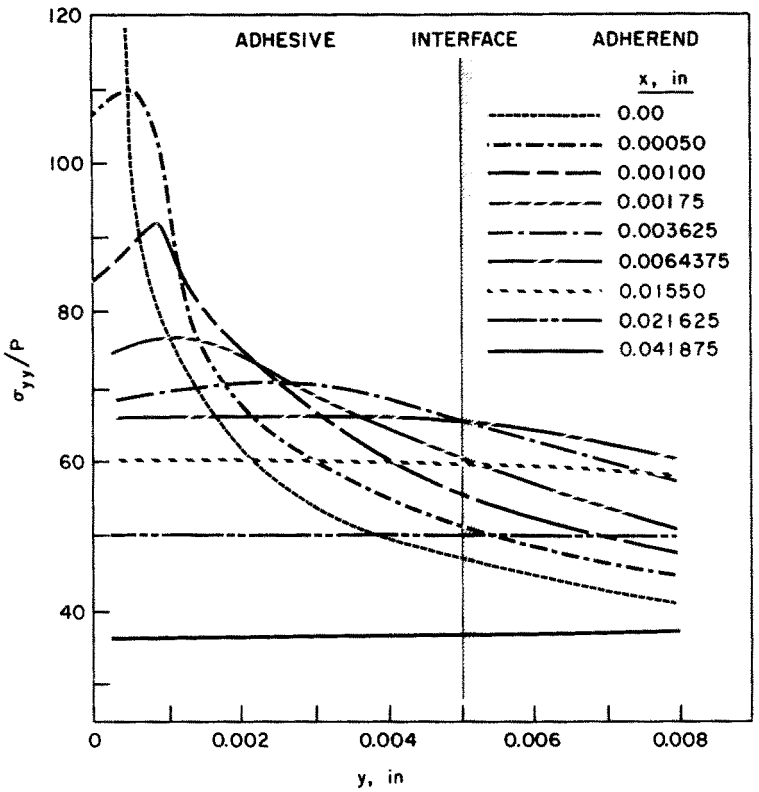

Figure 16. σ_{yy} along lines normal to the x-axis, DCB, $a = 2.0$ in, $t = 10$ mils, $E_2/E_1 = 20$.

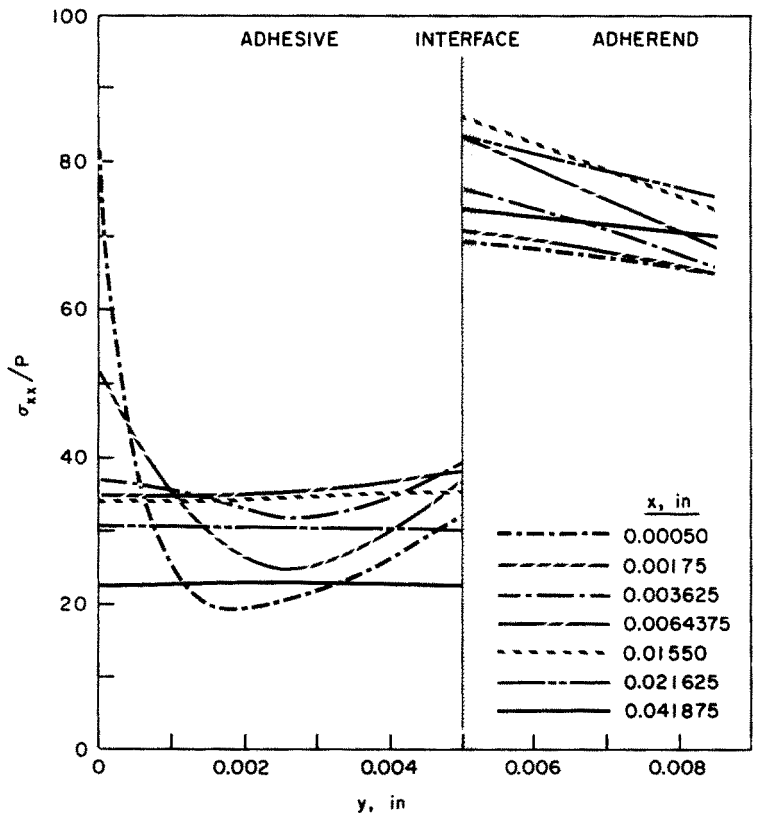

Figure 17. σ_{xx} along lines normal to the x-axis, DCB, $a = 2.0$ in, $t = 10$ mils, $E_2/E_1 = 20$.

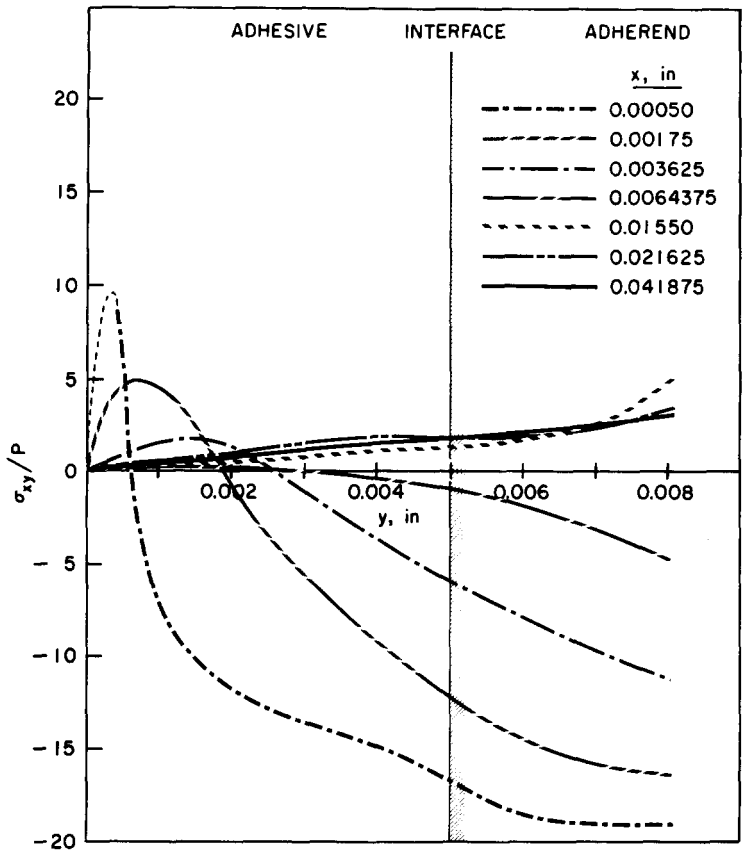

Figure 18. σ_{xy} along lines normal to the x-axis, DCB, $a = 2.0$ in, $t = 10$ mils, $E_2/E_1 = 20$.

tip. The stresses σ_{yy} and σ_{xy} are necessarily continuous across the interface, while σ_{xx} is discontinuous due to the change in elastic modulus (the corresponding strain is continuous). These figures demonstrate that the stress field within a distance of less than one adhesive thickness ahead of the crack tip is effectively uniform tension in the adhesive as it is stretched by the adherends. This is another indication of the localization of the crack tip disturbance in the adhesive system.

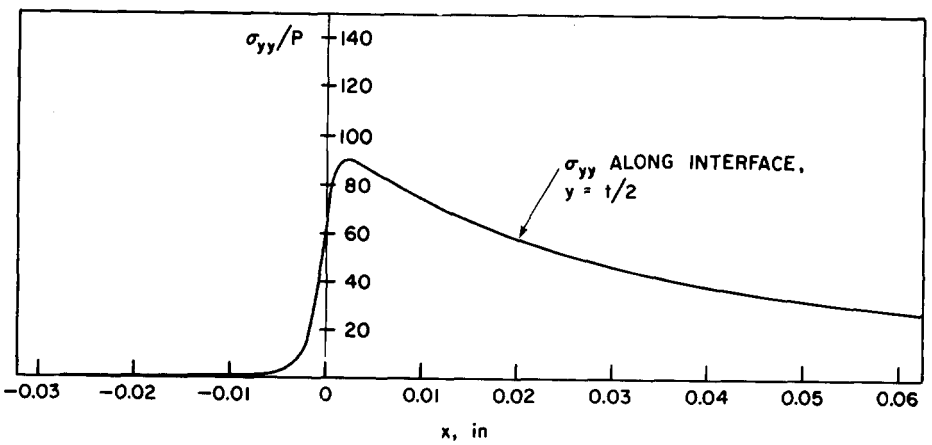

Figure 19. σ_{yy} along the interface, DCB, $a = 2.0$ in, $t = 10$ mils, $E_2/E_1 = 20$.

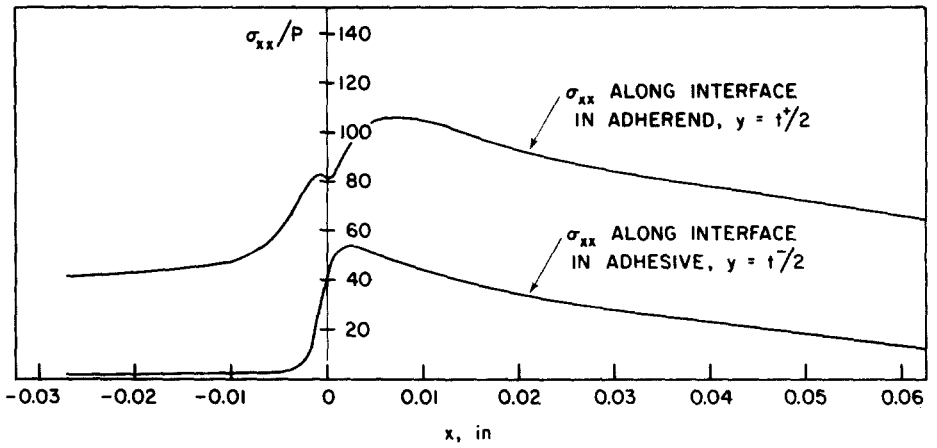

Figure 20. σ_{xx} along the interface, DCB specimen, $a = 2.0$ in, $t = 10$ mils, $E_2/E_1 = 20$.

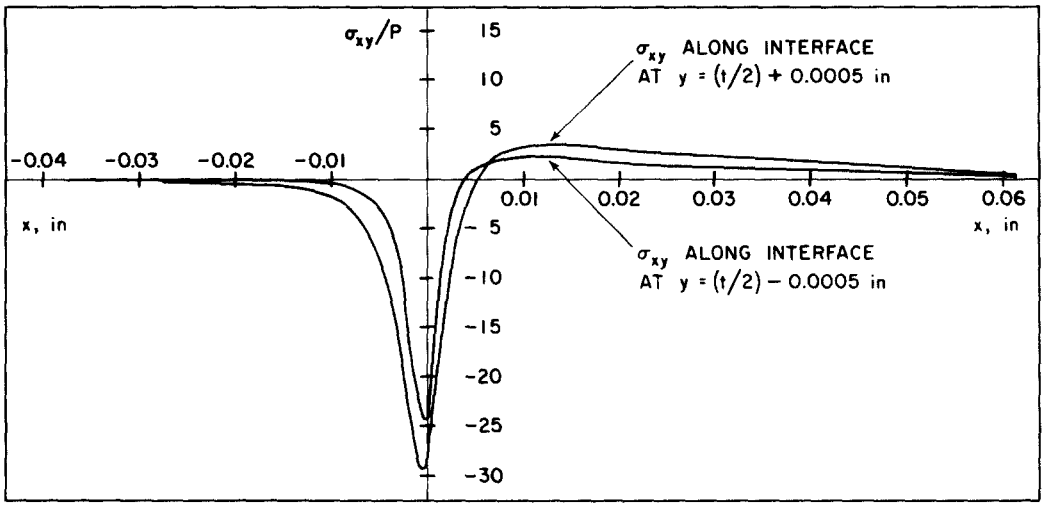

Figure 21. σ_{xy} along the interface, DCB specimen, $a = 2.0$ in, $t = 10$ mils, $E_2/E_1 = 20$.

Figures 19–21 give the stresses along the adhesive-adherend interface. In each case there is a rapid rise in the stress along the crack flank within one adhesive layer thickness of the crack tip. The stresses σ_{xx} and σ_{yy} peak just ahead of the crack tip, and then slowly decrease. The stress σ_{xy} peaks just before the crack tip and decreases rapidly ahead of it. While the stresses at the interface are concentrated near the crack tip, they are still significantly lower than those closer to the crack tip within the adhesive (Figs. 16–18).

It should be noted that the effects of residual stresses due to thermal contraction and the effects of the mismatch in Poisson's ratio at the interface on the stresses in the third direction have not been considered. These effects and inelastic behavior of the adhesive may be of great significance in actual adhesive bonded systems.

5. Summary and conclusions

An analysis based on the hybrid stress model of the finite element method and including a special crack tip element has been implemented and used to investigate the

stress distribution in a DCB-type adhesive fracture specimen. Results have been obtained for a range of adherend/adhesive modulus ratios and adhesive thicknesses to elucidate some fundamental characteristics of the problem. The only case considered is that of the crack embedded in the adhesive, although the crack may propagate close to the interface in some instances.

The stress field very close to the crack tip is found to be similar to that in monolithic systems. The stresses are singular and may be described by the conventional stress intensity factor and strain energy release rate. K_I and G_I are shown to be related through the adhesive modulus in the usual manner. Since G_I is determined primarily by the adherends, K_I is proportional to the square root of the adhesive modulus for a fixed adherend modulus. K_I is independent of adhesive thickness over the range studied due to the localization of the stress singular domain in the adhesive.

Significant differences from the monolithic case are observed in the stress field outside of a very limited region at the crack tip. The distance from the crack tip over which the singular behavior dominates is reduced in the adhesive case to a small fraction of the adhesive thickness, while the corresponding dimension for the monolithic case is the beam height. The stress field in the adherend is non-singular and is not characterized by the high stress gradients typical of a crack tip stress field. The stress field in the adhesive becomes nearly uniform at a distance of less than one adhesive layer thickness ahead of the crack tip.

Acknowledgement

Support for this work was provided by the American Cyanamid Company, to whom the authors are grateful.

REFERENCES

[1] E. J. Ripling, S. Mostovoy, and R. L. Patrick, *Adhesion, ASTM STP* 360 (1964) 5.
[2] E. J. Ripling and S. Mostovoy, *Journal of Adhesion*, 3 (1971) 107.
[3] J. J. Gillman, *Fracture*, B. L. Averbach, *et al.*, ed., MIT Press, Cambridge (1959) 193.
[4] Test No. D3433-75, Committee D-14 Recommended Practice, American Society for Testing and Materials (1976).
[5] T. H. H. Pian, *American Institute of Aeronautics and Astronautics Journal*, 2 (1964) 1333.
[6] T. H. H. Pian and P. Tong, *International Journal for Numerical Methods in Engineering*, 1 (1969) 3.
[7] P. Tong, T. H. H. Pian, and S. J. Lasry, *International Journal for Numerical Methods in Engineering*, 7 (1973) 297.
[8] N. I. Muskhelishvili, *Some Basic Problems in the Mathematical Theory of Elasticity*, Noordhoff, Groningen, The Netherlands (1953).
[9] O. L. Bowie, *Journal of Applied Mechanics, Transactions of ASME*, 34 (1964) 208.
[10] M. F. Kanninen, *International Journal of Fracture*, 9 (1973) 83.
[11] G. R. Irwin, *Journal of Applied Mechanics, Transactions of ASME*, 24 (1957) 361.
[12] S. Mostovoy, P. B. Crosley, and E. J. Ripling, *Journal of Materials*, 2 (1967) 661.
[13] G. G. Trantina, *Fracture Mechanics Approach to Adhesive Joints*, T. & A. M. Report No. 350, Dept. of Theo. and Appl. Mech., Univ. of Illinois (1971).

RÉSUMÉ

Le problème d'une éprouvette de rupture Double Poutre Cantilever comportant une liaison par adhésif fissurée a été analysée en utilisant un modèle de contrainte hybride et une analyse par élément fini qui incorpore un élément particulier à la pointe de la fissure. Les contraintes dans le champ proche et dans le champ éloigné ont été étudiées en fonction du rapport des modules de l'adhésif et de l'adhérent, et de l'épaisseur de l'adhésif. Les résultats sont comparés à un système monolitique en ce qui regarde le facteur d'intensité des contraintes et la localisation du domaine singulier des contraintes associé à l'extrémité de la fissure.